# Numerical Simulation of A Cubic Spout-Fluid Bed: Influences of Inlet Gas Temperature and Jet to Bed Cross-Section Ratio



doi: info:doi/10.1515/ijcre-2019-0144

**Ali Rahmani[1,2] / Mohsen Tamtaji[2] / Asghar Molaei Dehkordi[2]**

# Numerical Simulation of A Cubic Spout-Fluid Bed: Influences of Inlet Gas Temperature and Jet to Bed Cross-Section Ratio

[1] Okinawa Institute of Science and Technology Graduate University, Tancha, Okinawa, 904-0495 Kunigami-gun, Japan, E-mail: alirahmani@oist.jp
[2] Chemical and Petroleum Engineering, Sharif University of Technology, Tehran 11365, Iran (the Islamic Republic of), E-mail: alirahmani@oist.jp, tamtajimohsen2@gmail.com, amolaeid@sharif.edu

**Abstract:**
In this paper, we study the role of inlet gas temperature and jet to bed cross-section ratio on hydrodynamics and circulation patterns of particles in a spout-fluid bed. The system is modeled using CFD-TFM approach based on Eulerian-Eulerian method. Simulation results are validated by experimental data measured by (Link 2008. "PEPT and Discrete Particle Simulation Study of Spout-fluid Bed Regimes." *Aiche Journal* 54 (5): 1189–202). First, the sensitivity analysis of simulation results versus the most significant parameters are conducted to find the optimum values for each parameter. Subsequently, the role of inlet gas temperature and cross-section ratios are studied in detail. The simulation results clearly demonstrate that increasing the inlet gas temperature raises particles' velocity in the bed and affects the circulation pattern in annulus region. Additionally, it is shown that higher gas temperature leads to existence of hot spots in the annulus region. In case of jet to bed cross-section ratio, using larger ratios results in higher velocities and lower pressure drop along the bed.

**Keywords:** spout-fluid bed, inlet gas temperature, jet to bed cross-section ratio

**DOI:** 10.1515/ijcre-2019-0144

**Received:** August 17, 2019; **Revised:** January 28, 2020; **Accepted:** February 10, 2020

## 1 Introduction

Nowadays, spout-fluid beds due to the enhancement of gas-solid mass and heat transfer rates have been found a wide range of applications from electrochemical reactors (Walsh and de Leon 2018) to pharmaceutical materials drying (de Freitas 2019). The enhancement originates from higher background gas flow in spout-fluid bed which results in higher circulation and mixing rates of solid particles. Generally, spout-fluid beds contain three regions called spout, annulus, and fountain where circulation patterns of the solid particles and fluid dynamic properties in these regions vary widely. In this regard, recently savari et al. have studied several parameters affecting the stability of spout-fluid beds (Savari et al. 2019).

In addition to these parameters, other factors impact the efficiency of the bed and should be investigated. Several researchers were exploited computational fluid dynamic (CFD) techniques to simulate spout-fluid beds and study the most significant parameters on the in spout-fluid beds in both 2D and 3D frameworks. For instance, Yang et al. studied fluid behavior, velocity distribution, and solid phase concentration with different tube configurations to evaluate effect of the inlet geometry on the performance of the system for a cylindrical column (Yang et al. 2013). Additionally, some researchers studied variations of spout region boundaries during spout-fluid beds scale up in beds with other geometries (Du et al. 2013; Zhong et al. 2013). Furthermore, influence of bed geometry on operating pressure drop, minimum spouting velocity, and flow patterns were studied by several researchers (Saidi, Tabrizi, and Grace 2019).

Another significant parameter affecting the gas-solid interactions in the bed is temperature distribution along the bed which can be controlled by different methods. For instance, Wu et al. studied effect of temperature on the pressure drop, background gas velocity, minimum spouting velocity, and flow pattern in a conical spout-fluid bed (Wu et al. 2019). In another attempt, Correia et al. measured thermal profile at different locations in the bed and showed that temperature distribution in different regions was reduced with increasing the gas flow in a conical spout-fluid bed (Correia et al. 2019). In case of flat bottom spouted beds, some researchers tried to use CFD-DEM approach to evaluate temperature distribution in the chamber, however they mostly

**Ali Rahmani, Asghar Molaei Dehkordi** are the corresponding authors.

modeled their systems in 2D frameworks. For example, Wang et al. studied configurational temperature and translational and rotational granular temperatures of particles in a flat bottom spout-fluid bed in 2D framework (Wang et al. 2014). They successfully showed that the configurational temperature is larger and the rotational and translational granular temperatures are smaller at higher solid volume fraction.

In this paper, we want to study effects of the inlet gas temperature and jet to bed cross-section ratio on the hydrodynamics of the flow in a flat bottom spout-fluid bed in 3D framework by CFD-TFM approach. However, TFM model cannot capture discrete nature of the solid phase less computational resources are needed. For accurate simulation parameters it can provide reliable approximation for the hydrodynamics of the large systems. This work has the potential to complement the previous analysis in literature trying to investigate role of jet to bed cross-section ratio and temperature distribution in flat bottom spout-fluid beds (note that by the jet to bed cross-section ratio we mean the ratio between overall surface of the nozzle to the total surface of the bed cross section).

In what follows, first we introduce the geometry of the spout-fluid bed and define initial and boundary conditions. Subsequently, we present the conservation and constitutive equations used in the simulation. Then, we specify the simulation conditions and the numerical method applied to solve the governing equations. Finally, we present the results of the simulations and compare them with the experimental data measured by (Link et al. 2008).

## 2 Governing equations and simulation conditions

### 2.1 Governing equations

In TFM model, solid particles are considered as a continuous phase like fluids. Mass, momentum, energy, and transportation of granular temperature equations used in kinetic theory of granular flow (KTGF) are solved simultaneously using Ansys-Fluent. Some of the drag models are added to the main setup as a user define function (UDF) developed in C language. Solution of these coupled equations results in determination of velocity and temperature fields in the spout-fluid bed.

#### 2.1.1 Conservation equations

The overall conservation of mass for gas (g) and solid (s) phases are

$$\frac{\partial\left(\varepsilon_{\mathrm{g}}\rho_{\mathrm{g}}\right)}{\partial \mathrm{t}}+\nabla.\left(\varepsilon_{\mathrm{g}}\rho_{\mathrm{g}}\mathbf{v_g}\right)=0 \tag{1}$$

$$\frac{\partial\left(\varepsilon_{\mathrm{s}}\rho_{\mathrm{s}}\right)}{\partial \mathrm{t}}+\nabla.\left(\varepsilon_{\mathrm{s}}\rho_{\mathrm{s}}\mathbf{v_s}\right)=0 \tag{2}$$

where $\mathbf{v_g}$, $\mathbf{v_s}$, $\varepsilon_{\mathrm{g}}$, $\varepsilon_{\mathrm{s}}$, $\rho_{\mathrm{g}}$, and $\rho_{\mathrm{s}}$ are the gas velocity, solid velocity, volume fraction of gas phase, volume fraction of solid phase, gas density, and the solid density, respectively.

Conservation of momentum for gas and solid phases can be expressed as

$$\frac{\partial\left(\varepsilon_{\mathrm{g}}\rho_{\mathrm{g}}\mathbf{v_g}\right)}{\partial \mathrm{t}}+\nabla.\left(\varepsilon_{\mathrm{g}}\rho_{\mathrm{g}}\mathbf{v_g}\mathbf{v_g}\right)=-\varepsilon_{\mathrm{g}}\nabla \mathrm{P_g}+\nabla.\overline{\overline{\tau}}_{\mathrm{g}}+\varepsilon_{\mathrm{g}}\rho_{\mathrm{g}}\mathbf{g}-\mathbf{R_{gs}} \tag{3}$$

$$\frac{\partial\left(\varepsilon_{\mathrm{s}}\rho_{\mathrm{s}}\mathbf{v_s}\right)}{\partial \mathrm{t}}+\nabla.\left(\varepsilon_{\mathrm{s}}\rho_{\mathrm{s}}\mathbf{v_s}\mathbf{v_s}\right)=-\varepsilon_{\mathrm{s}}\nabla \mathrm{P_s}+\nabla.\overline{\overline{\tau}}_{\mathrm{s}}+\varepsilon_{\mathrm{s}}\rho_{\mathrm{s}}\mathbf{g}+\mathbf{R_{gs}} \tag{4}$$

where $\mathrm{P_g}$, $\mathrm{P_s}$, $\mathbf{g}$, $\mathbf{R_{gs}}$, $\overline{\overline{\tau}}_{\mathrm{g}}$, and $\overline{\overline{\tau}}_{\mathrm{s}}$ are the gas pressure, solid phase pressure, gravity constant, phase interaction forces, and stress tensor for the gas and solid phases, respectively.

Granular temperature is proportional to the kinetic energy of random movements of the particles and can be evaluated by (Agrawal et al. 2001).

$$\frac{3}{2}\left[\frac{\partial\left(\varepsilon_{\mathrm{s}}\rho_{\mathrm{s}}\theta_{\mathrm{s}}\right)}{\partial \mathrm{t}}+\nabla.\left(\varepsilon_{\mathrm{s}}\rho_{\mathrm{s}}\mathbf{v_s}\theta_{\mathrm{s}}\right)\right]=-\left(\mathrm{P_s}\bar{\bar{\mathrm{I}}}+\overline{\overline{\tau}}_{\mathrm{s}}\right):\nabla\mathbf{v_s}+\nabla.\left(\mathrm{k}_{\theta\mathrm{s}}\nabla\theta_{\mathrm{s}}\right)-\gamma\theta_{\mathrm{s}}+\varphi_{\mathrm{gs}} \tag{5}$$

To determine the temperature distribution in the spout-fluid bed, energy balance is considered for both gas and solid phases (Behjat, Shahhosseini, and Hashemabadi 2008)

$$\varepsilon_g \rho_g C_{Pg} \left( \frac{\partial T_g}{\partial t} + \mathbf{v_g}.\nabla T_g \right) = - \left( H_g + \Delta H_{rg} \right) \tag{6}$$

$$\varepsilon_s \rho_s C_{Ps} \left( \frac{\partial T_s}{\partial t} + \mathbf{v_s}.\nabla T_s \right) = - \left( H_s + \Delta H_{rs} \right) \tag{7}$$

where $C_{Pg}$, $C_{Ps}$, $H_g = -\gamma_g \left( T_s - T_g \right)$, $H_s$, $H_{rg}$, and $H_{rs}$ represent specific heat of gas phase, specific heat of solid phase, heat transfer from gas to solid phase, heat transfer from solid to gas phase, reaction heat in gas phase, and reaction heat in solid phase, respectively. The heat transfer coefficient in the bed is function of Nusselt number and can be derived as

$$\gamma_g = \frac{6 k_g \varepsilon_s Nu}{d_s^2} \tag{8}$$

$$Nu = (7 - 10\varepsilon_g + 5\varepsilon_g^2)(1 + 0.7 Re^{0.2} Pr^{\frac{1}{3}}) + (1.33 - 2.4\varepsilon_g + 102\varepsilon_g^2 Re^{0.7} Pr^{\frac{1}{3}}) \tag{9}$$

### 2.1.2 Constitutive equations

To determine both velocity and temperature profile in the system by (1) to (9), other parameters should be specified through several constitutive equations.

Generally, the solid phase pressure $P_s$ can be derived by (Agrawal et al. 2001)

$$P_s = \varepsilon_s \rho_s \theta_s + 2\rho_s (1 + e_{ss}) \varepsilon_s^2 g_{0,ss} \theta_s \tag{10}$$

where $\theta_s$, $e_{ss}$, and $g_{0,ss}$ denote the granular temperature, restitution coefficient for particle-particle collisions, and the solid radial distribution function, respectively. Radial distribution function can be obtained from (Carnahan and Starling 1969)

$$g_{0,ss} = \frac{1}{1 - \varepsilon_s} + \frac{3\varepsilon_s}{2(1 - \varepsilon_s)^2} + \frac{\varepsilon_s^2}{2(1 - \varepsilon_s)^3} \tag{11}$$

moreover, the stress tensor for the solid phase can be evaluated as follows (Carnahan and Starling 1969)

$$\bar{\bar{\tau}}_s = \left( -P_s + \frac{1}{2} (1 + e_{ss}) \mu_b \nabla.\mathbf{v_g} \right) \bar{\bar{I}} + 2\mu_s S_s \tag{12}$$

$$S_s = \frac{1}{2} \left( \nabla \mathbf{v_s} + (\nabla \mathbf{v_s})^T \right) - \frac{1}{3} \nabla.\mathbf{v_s} \bar{\bar{I}} \tag{13}$$

$$\mu_b = \frac{256}{5\pi} \mu \varepsilon_s^2 g_{0,ss} \tag{14}$$

where $\mu_b$, $\mu_s$, and $\mu$ are the bulk, solid tension, and granular viscosities, respectively. The stress tensor for the gas phase can be calculated by (15) to (20)

$$\bar{\bar{\tau}}_g = 2\mu_{gt} S_g \tag{15}$$

$$S_g = \frac{1}{2}\left(\nabla \mathbf{v_g} + \left(\nabla \mathbf{v_g}\right)^T\right) - \frac{1}{3}\nabla.\mathbf{v_g}\bar{\bar{I}} \tag{16}$$

$$\mu_{gt} = \mathrm{Min}\left(\mu_{Max}, \mu_g + \mu_e\right) \tag{17}$$

$$\mu_e = 2l_s^2 \varepsilon_g \rho_g \sqrt{I_{2Dg}} \tag{18}$$

$$I_{2Dg} = \frac{1}{6}\left[\left(D_{g,11} - D_{g,22}\right)^2 + \left(D_{g,22} - D_{g,33}\right)^2 + \left(D_{g,33} - D_{g,11}\right)^2\right] + D_{g,12}^2 + D_{g,23}^2 + D_{g,31}^2 \tag{19}$$

$$D_g = \frac{1}{2}\left(\nabla \mathbf{v_g} + \left(\nabla \mathbf{v_g}\right)^T\right) \tag{20}$$

where $\mu_{gt}$, $\mu_g$, $\mu_e$, $l_s$, $I_{2Dg}$, and $D_{g,ij}$ are the turbulent viscosity of gas phase, gas viscosity, eddy viscosity of gas phase, turbulent length scale parameters, second invariant of the strain rate tensor for gas phase, and the rate of strain tensor for fluid phase, respectively.

In eq. (5), $-P_s\bar{\bar{I}} + \bar{\bar{\tau}}_s$ is the generation of solid tension, $k_{\theta s}\nabla\theta_s$ is the energy diffusion, and $k_{\theta s}$ is the diffusion coefficient. In addition, in (5) $\gamma\theta_s$ demonstrates the energy dissipation because of collisions and $\varphi_{gs}$ illustrates the energy dissipation between solid and gas phases. In the present work, $k_{\theta s}$ is calculated by (Gamwo et al. 2003)

$$k_{\theta s} = \frac{150\rho_s d_s\sqrt{\theta_s \pi}}{384\left(1 + e_{ss}\right) g_{0,ss}}\left[1 + \frac{6}{5}\varepsilon_s g_{0,ss}\left(1 + e_{ss}\right)^2 + 2\rho_s \varepsilon_s^2 d_s\left(1 + e_{ss}\right) g_{0,ss}\right] \tag{21}$$

and $\gamma\theta_s$ can be calculated by the correlation presented by (Lun et al. 1984)

$$\gamma\theta_s = \frac{12\left(1 - e_{ss}^2\right) g_{0,ss}}{d_s\sqrt{\pi}}\rho_s \varepsilon_s^2 \theta_s^{\frac{3}{2}} \tag{22}$$

$$\varphi_{gs} = -3k_{gs}\theta_s \tag{23}$$

Generally, in the TFM approach a viscosity is defined for the solid phase considering contribution of shear and bulk viscosities due to the transformation or collisional movements.

$$\mu_s = \mu_{s,col} + \mu_{s,kin} + \mu_{s,fr} \tag{24}$$

where $\mu_{s,fr}$, $\mu_{s,kin}$, and $\mu_{s,col}$ are the frictional, kinetic, and collisional viscosities, respectively. Solid phase shear viscosity can be calculated considering contribution of collisional and kinetic terms (Santos, Murata, and Barrozo 2009).

$$\mu_{s,col} = \frac{\varepsilon_s d_s \rho_s \sqrt{\theta_s \pi}}{6\left(3 - e_{ss}\right)}\left[1 + \frac{2}{5}\left(1 + e_{ss}\right)\left(3e_{ss} - 1\right)\varepsilon_s g_{0,ss}\right] \tag{25}$$

$$\mu_{s,kin} = \frac{10\varepsilon_s d_s \rho_s \sqrt{\theta_s \pi}}{96\varepsilon_s\left(1 + e_{ss}\right) g_{0,ss}}\left[1 + \frac{4}{5}\left(1 + e_{ss}\right)\varepsilon_s g_{0,ss}\right]^2 \tag{26}$$

Another parameter related to the viscosity is bulk granular viscosity that exhibits particles resistance against expansion and contraction during fluidization (Lun et al. 1984).

$$\lambda_s = \frac{4}{3}\varepsilon_s \rho_s d_s g_{0,ss}\left(1 + e_{ss}\right)\left(\frac{\theta_s}{\pi}\right)^{0.5} \tag{27}$$

Frictional viscosity considers viscoelastic behavior of the solids. It becomes be dominant where solid phase reaches its maximum volume fraction and can be calculated by (Schaeffer 1987).

$$\mu_{s,fr} = \frac{P_s \sin\emptyset}{2\sqrt{I_{2D}}} \tag{28}$$

Where $P_s$ and $\emptyset$ are solid pressure and internal frictional angle, respectively. If solid phase reaches the packing limit, the solid pressure becomes large according to specified radial distribution function and (29) has been proposed by (Johnson and Jackson 1987)

$$P_s = \frac{C_D Re_s \varepsilon_s}{24 v_{rs}^2} \tag{29}$$

where $C_D$ and $v_{rs}$ are the drag coefficient and terminal velocity of solid phase at operating conditions of the bed, respectively.

## 2.2 Simulation condition

A schematic diagram of the bed is shown in Figure 1. Solid particles diameter is 4.04 mm and their density is 2526 kg/m$^3$. Air is used as the spouting agent and is introduced with a uniform velocity 60 m/s from the bottom of the bed and the background velocity is 2.5 m/s. At the walls, no-slip boundary condition is assumed for the gas and Johnson-Jackson slip boundary condition is used for solid phase (Johnson and Jackson 1987). The specularity coefficient used in this work is 0.5 and the restitution coefficient of the solid particles is 0.95. The boundary condition for the outlet of spout-fluid bed is atmospheric pressure. The initial bed height is 0.195 m with uniform solid volume fraction of 0.6.

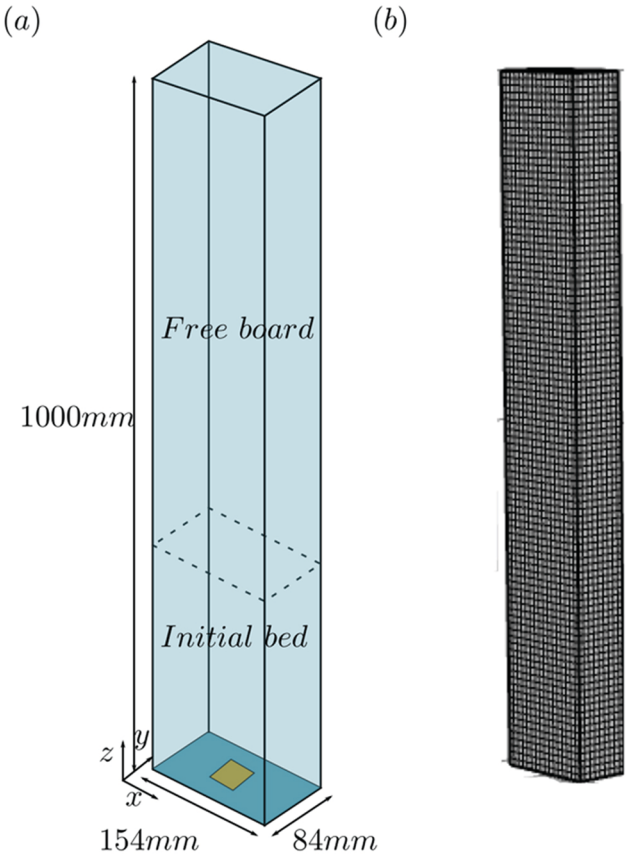


**Figure 1:** (a) Schematic of a cubic spout-fluid bed and a positively oriented orthonormal basis placed at the bottom of the bed. (b) Structured mesh grids.

The dimensions of the bed are selected according to the work by (Link et al. 2008). Conservation equations of mass, momentum, energy, and granular temperature are solved by means of finite volume method. SIMPLE method is chosen for coupling of pressure and velocity. First-order implicit time discretization and second-order upwind spatial discretization are used for the conservation of mass, momentum, energy, and granular temperature equations. Time step is adjusted at $10^{-5}$ s and maximum number of iterations in each step is set to be 60.

# 3 Results and Discussion

In this work, sensitivity analysis of the simulation results to drag force, specularity, restitution, and friction coefficients on hydrodynamics of the spout-fluid bed are studied. Subsequently, effects of jet to bed cross-section ratio and inlet gas temperature are discussed in detail.

## 3.1 Mesh independency

Figure 2 shows the average voidage from 10 s to 25 s versus height of the bed for three mesh sizes i. e. Mesh 1=17×10×80, Mesh 2=19×12×90, and Mesh 3=21×14×100 (number of discretization are based on, respectively x × y × z coordinates). The mesh number of 19 × 12 × 90 is selected for the simulation to obtain the most accurate result.

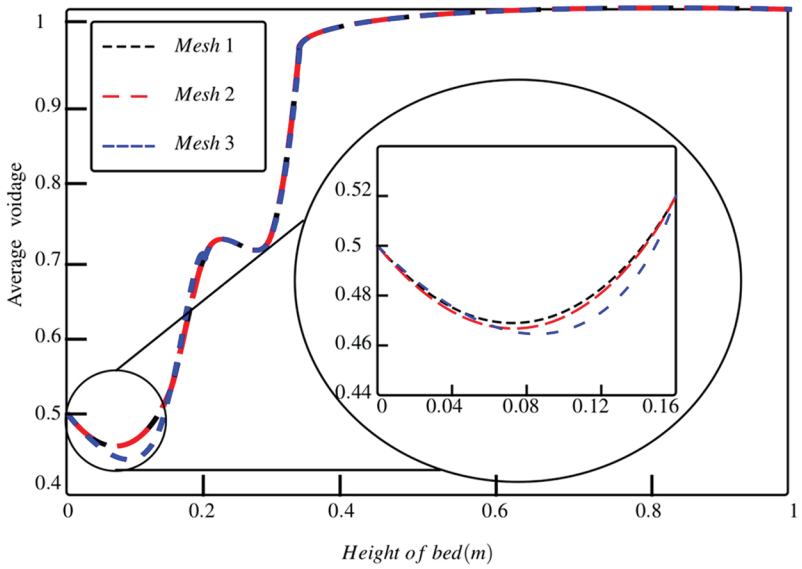


**Figure 2:** Mesh independency study using average voidage along the bed for three different mesh sizes (Mesh 1=17 × 10 × 80, Mesh 2=19 × 12 × 90, and Mesh 3=21 × 14 × 100 based on **x** × **y** × **z**).

## 3.2 Sensitivity analysis of numerical results to drag models, specularity, restitution, and friction coefficients

Figure 3 demonstrates the time-averaged velocity profile along z direction at z = 0.15 m and z = 0.25 m for several drag models (see Table 1) and the experimental measurements by (Link et al. 2008). The existence of spout and annulus regions can be clearly predicted by all models. However, in the spout region where the gas velocity is high Wen-Yu and Gidaspow models can predict the experimental results more accurately. This situation can be explained considering the fact that for Wen-Yu model, it can predict drag forces in dilute system precisely, the system that voidage is greater than 0.9. In the system evaluated here, the condition is satisfied as the voidage is very high in spout region. Therefore, the velocity profile can be specified accurately by Wen-Yu model. In case of Gidaspow model as it is depicted in Table 1, the model is combination of Ergun and Wen-Yu models where at high voidage it converges to Wen-Yu model. Therefore, Gidaspow model can predict the experimental results precisely.

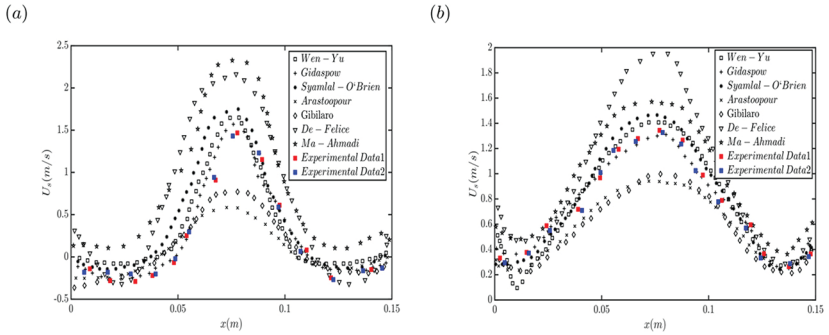


**Figure 3:** Z-component of particle velocity using various drag models and the corresponding experimental data at (a) z = 0.15 m, and (b) z = 0.25 m. Experimental data 1 and 2 represent the measurments obtained separately at the University of Twente in the Netherlands and the University of Birmingham in the United Kingdom, respectively (Link et al. 2008).

**Table 1:** Summary of momentum exchange models used in simulation setups.

| **Momentum exchange coefficient models** | |
|---|---|
| **Wen-Yu model** | |
| $k_{gs} = \frac{3}{4} C_D \frac{\rho_g \varepsilon_g \varepsilon_s \lvert \mathbf{v_g} - \mathbf{v_s} \rvert}{d_s} \varepsilon_g^{-2.65}$ | (T1-1) |
| $C_D = \frac{24}{\varepsilon_g Re_s} \left[ 1 + 0.15 (\varepsilon_g Re_s)^{0.687} \right]$ | |
| $Re_s = \frac{\rho_g \lvert \mathbf{v_g} - \mathbf{v_s} \rvert d_s}{\mu_g}$ | |
| **Huilian-Gidaspow model** | |
| $k_{gs} = \psi k_{gs,\,Ergun} + (1 - \psi)\, k_{gs,\,Wen-Yu}$ | (T1-2) |
| $\psi = \frac{1}{2} + \frac{\arctan(262.5(\varepsilon_s - 0.2))}{\pi}$ | |
| **Syamlal-O'Brien model** | |
| $k_{gs} = \frac{3}{4} C_D \frac{\rho_g \varepsilon_g \varepsilon_s \lvert \mathbf{v_g} - \mathbf{v_s} \rvert}{V_{rs}^2 d_s}$ | (T1-3) |
| $C_D = \left( 0.63 + 4.8 \sqrt{\frac{V_{rs}}{Re_s}} \right)^2$ | |
| $V_{rs} = 0.5 \left( A - 0.06 Re_s + \sqrt{(0.06 Re_s)^2 + 0.12 Re_s (2B - A) + A^2} \right)$ | |
| $Re_s = \frac{\rho_g \lvert \mathbf{v_g} - \mathbf{v_s} \rvert d_s}{2 \mu_g}$ | |
| $A = \varepsilon_g^{4.14}$ | |
| $B = \begin{cases} 0.8 \varepsilon_g^{1.28} & \varepsilon_g \leq 0.85 \\ \varepsilon_g^{2.65} & \varepsilon_g > 0.85 \end{cases}$ | |
| **Gibilaro model** | |
| $k_{gs} = \left( \frac{17.3}{Re_s} + 0.336 \right) \rho_g \frac{\lvert \mathbf{v_g} - \mathbf{v_s} \rvert}{d_s} \varepsilon_s \varepsilon_g^{-1.8}$ | (T1-4) |
| $Re_s = \frac{\rho_g \varepsilon_g \lvert \mathbf{v_g} - \mathbf{v_s} \rvert d_s}{2 \mu_g}$ | |
| **Ma-Ahmadi model** | |
| $k_{gs} = 18 \frac{\mu_g \varepsilon_s}{d_s^2} \left( \frac{\varepsilon_g}{\varepsilon_s} \right)^{-2.5 \varepsilon_s} \left( 1 + Re_s^{0.75} \right)$ | (T1-5) |
| $Re_s = \frac{\varepsilon_g \rho_g \lvert \mathbf{v_g} - \mathbf{v_s} \rvert d_s}{\mu_g}$ | |
| **Di Felice model** | |
| $k_{gs} = \frac{3}{4} \frac{C_D \varepsilon_s \varepsilon_g \rho_g}{d_s} \lvert \mathbf{v_g} - \mathbf{v_s} \rvert \varepsilon_g^{-\eta}$ | (T1-6) |
| $\eta = 3.7 - 0.65 \exp \left[ -\frac{1}{2} (1.5 - \log (Re_s))^2 \right]$ | |
| $C_D = \left( 0.63 + 4.8 \sqrt{\frac{1}{Re_s}} \right)^2$ | |
| $Re_s = \frac{\varepsilon_g \rho_g \lvert \mathbf{v_g} - \mathbf{v_s} \rvert d_s}{\mu_g}$ | |
| **Arastoopour model** | |
| $k_{gs} = \left( \frac{17.3}{Re_s} + 0.336 \right) \rho_g \frac{\lvert \mathbf{v_g} - \mathbf{v_s} \rvert}{d_s} \varepsilon_s \varepsilon_g^{-2.8}$ | (T1-7) |
| $Re_s = \frac{\varepsilon_g \rho_g \lvert \mathbf{v_g} - \mathbf{v_s} \rvert d_s}{\mu_g}$ | |

The other model is Syamlal-O'Brien which according to Figure 3 shows some discrepancy with the experimental measurements. It can be explained possibly by the fact that this model uses terminal velocity of particles to determine the minimum spouting velocity. So, the computed values for momentum exchange may vary with minimum spouting condition. The other models are Gibilaro, Arastoopour, Di Felice, and Ma-Ahmadi (Du et al. 2006; Duangkhamchan et al. 2010). As it is shown in Figure 3, Gibilaro and Arastoopour models underestimate the z-component of the velocity profile in spout regions where the drag forces exerted to the particles are large. De-Felice and Ma-Ahmadi drag models predict the z-component of velocity field larger than its real values and the main reason is higher drag coefficients calculated by these two models. For regions near the walls where the voidage is small, the models which consider particle-particle interactions better give more accurate results. Comparing Figure 3(a) and (b) shows that at higher elevations in the bed where the gas velocity is smaller and the particles concentration is higher, the velocity profile becomes wider and the difference between maximum and minimum of the velocity becomes smaller. In this situation, still Gidaspow drag model gives the best approximation of the experimental measurements. Hence, the Goidaspow model is used in this work to predict the drag forces exerted to particles in all regions of the spout-fluid bed. This results is consistent with the sensitivity analysis reported by Moliner et al., they showed that Gidaspow model can predict the hydrodynamics of the spout-fluid bed better. Although, they showed that depending on the size of the bed and solid volume fraction other drag models may give reasonable predictions (Moliner et al. 2019).

Besides of drag models, there are several other parameters affecting the simulation results among the most important ones are specularity, restitution, and friction coefficients. The specularity coefficient represents the wall smoothness in a sense that $\varphi = 0$ and $\varphi = 1$ denote ideal smooth and rough walls, respectively. To study effect of specularity coefficient on z-component velocity profile of the particles three values are examined. According to Figure 4(a), specularity coefficient influences the velocity profile in the bed and the most appropriate value is 0.1. However, its significance is not as crucial as the case reported by (Fattahi, Hosseini, and Ahmadi 2016). The possible explanation may come from the fact that in this work the thickness of the bed is comparable with the width.

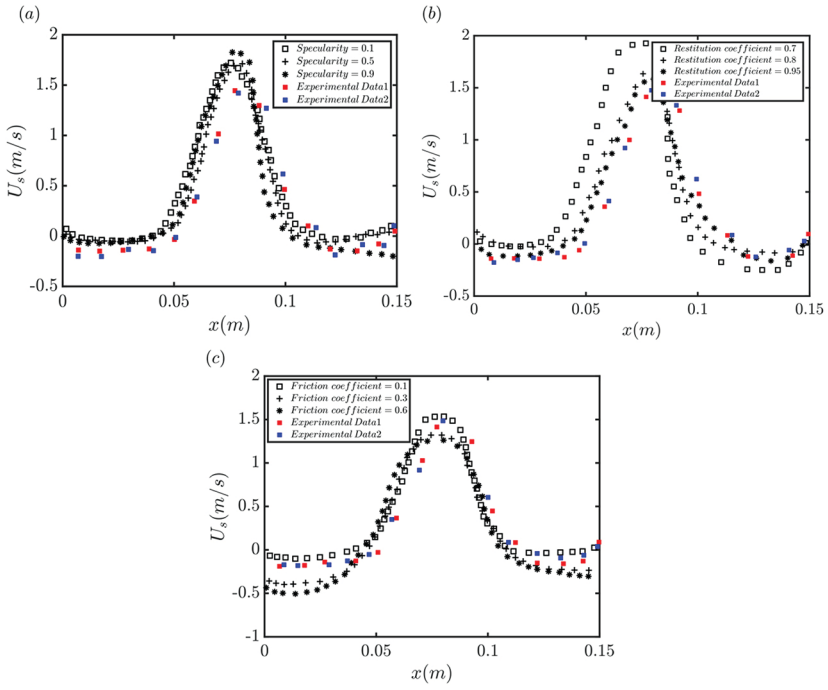


**Figure 4:** Sensitivity analysis of the numerical results with respect to (a) specularity, (b) restitution, and (c) friction coefficients in the model at z = 0.15 m.

In case of restitution coefficient several values ($e_{ss} = 0.7, 0.8, 0.95$) are exploited (see Figure 4(b)). Smaller coefficients correspond to more loss of momentum. It is observed that simulation results are sensitive to values of this coefficient since TFM model uses some properties such as bulk viscosity and solid shear viscosity which depend strongly on this parameter. In all cases studied in this work, the restitution coefficient is set to 0.95 as it predicts the experimental results better. Previously, Hosseini et al. showed that the role restitution coefficient is negligible in 2D framework. Although, it became important for the case of 3D simulations as the losses on the back and front walls significantly impact the 3D results (Hosseini, Fattahi, and Ahmadi 2015). This result is compatible with our 3D simulation results of the spout-fluid bed. The other parameter influencing the particles motion in the bed is friction factor. Figure 4(c) shows that increasing the friction factor leads to smaller

particles velocity. Recently, Wang et al. has shown that augmenting friction coefficient results in lower particle velocity. Because, more energy dissipates from particle collisions in the bed (Wang et al. 2018). This argument is consistent with what we obtain from our simulation results. In this study, the friction factor is set to 0.1 which gives the best fit to experimental measurements.

The discrepancy between the simulation and experimental data may originate from particle size distribution, particle-particle or particle-wall interactions, and variation of physical properties as a function of temperature. In this study, we assume that all particles diameter is 4.04 mm, however in reality there is a size distribution for the particles used in the experiment. Additionally, the particle-particle and particle-wall interactions cannot be captured entirely as in TFM formulation the solid phase treated as a continuous phase. Besides, the assumption that fluid properties in each computational domain is constant may not match the reality, especially in the spout region and around the gas inlet where the gas velocity is high and even small changes in gas density may lead to a large difference in drag forces.

### 3.3 Effect of jet to bed cross-section ratio

To evaluate effects of jet to bed cross-section on hydrodynamics of the spout-fluid bed, four different ratios are examined. Figure 5 depicts z-component of particles velocity at $z = 0.15$ m and $z = 0.25$ m. By reducing the inlet jet cross-section while inlet gas velocity remains constant, particles velocity reduces and this trend is much more significant in spout zone where the particles experience higher acceleration. Besides, at $Sj/St = 0.05$ the drag force exerted on the particles cannot spout the particles and bubbling regime appears in the bed. Comparing Figure 5(a) and (b) shows that at higher elevations in the bed, increasing the nozzle area do not necessarily leads to higher velocities. In a sense that at $z = 0.25$ m, $Sj/St = 0.143$ represents higher velocities. This phenomenon can be explained by the fact that at higher elevation for large nozzles the gas move through the particles from several channels and the forces exerted to them reduces, hence the overall velocity of particles reduces across the bed.

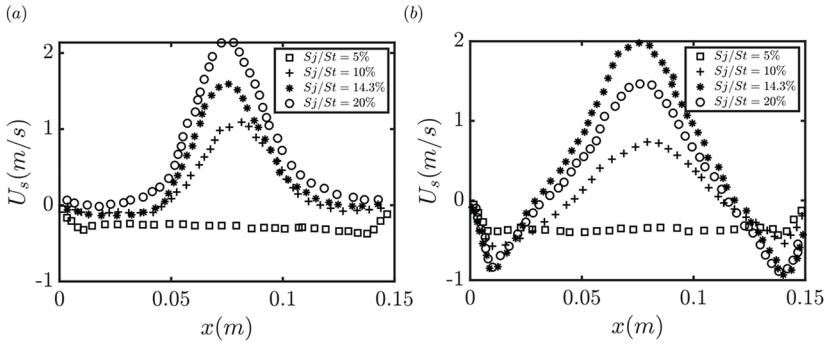


**Figure 5:** Effect of jet to bed cross-section ratio on the z-component of particles velocity at (a) $z = 0.15$ m and (b) $z = 0.25$ m.

In addition to the velocity field, jet to bed cross-section ratio influences pressure drop along the bed significantly. Figure 6 demonstrates pressure drop along the center line in the bed for four different ratios. Figure 6(a) shows that pressure fluctuations for $Sj/St = 0.05$ is constant and approximately it is placed in range of 2900–4800 Pa. By increasing the jet to bed cross-section ratio, it can be observed that fluctuations amplitude decreases in a way that pressure drop for $Sj/St = 0.2$ reaches 2935 Pa and unstable bubbling regime appears in the bed. Another crucial point is that by increasing the jet cross-section, the pressure drop along the bed becomes unstable, as it is shown in Figure 6(d). This behavior may be explained by considering the fact that larger jet cross section leads to existence of several side channels for gas phase especially at higher elevations where the gas velocity decline due to momentum exchange with solid phase.

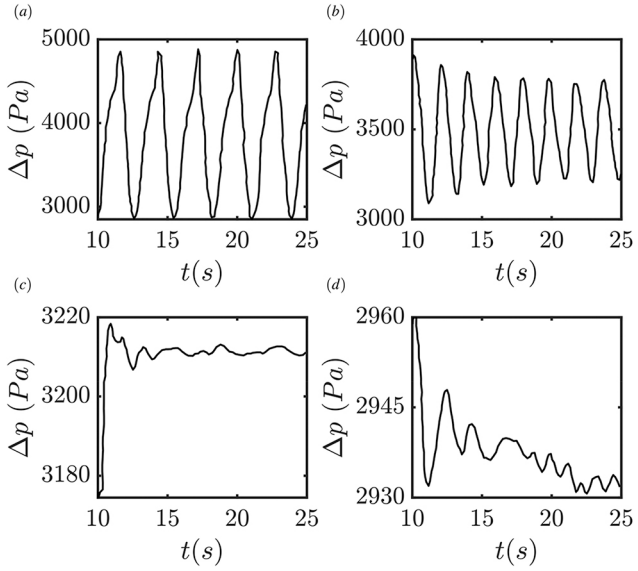


**Figure 6:** Effect of jet to bed cross-section ratio on pressure drop along the bed at (a) Sj/St = 5 %, (b) Sj/St = 10 %, (c) Sj/St = 14.3 %, and (d) Sj/St = 20 %.

Figure 7 shows the solid volume fraction in the bed for four different ratios. In Figure 7(a) where Sj/St = 0.05, three common regions in the spout-fluid bed i. e. spout, annulus, and fountain cannot be recognized clearly. Because, insufficient drag force cannot compensate the gravitational forces in the bed and the gas phase is distributed homogeneously at each cross-section. Figure 7(b) and (c) demonstrate particle volume fraction distribution at z = 0.25 m and z = 0.15 m, respectively. At z = 0.25 m the three main regions cannot be distinguished and the particle volume fraction is approximately constant across the bed (see Figure 7(b)). By increasing the cross-sections ratio, the boundaries between spout, annulus, and fountain will appear and the maximum particle volume fraction can be found in the middle of the bed. Moreover, it is worth to note that increasing Sj/St augments the fountain region. Figure 7(c) shows particle volume fraction at z = 0.15 m. In this elevation, most of the particles remain in regions near the walls because of larger gas velocity. Figure 7(d) illustrates the particle volume fraction along the bed at x = 0.075 m, according to this figure by increasing the cross-sections ratio maximum particle volume fraction moves to higher elevations in the bed and particles are carried to higher levels. This result is consistent with the study reported by (Setarehshenas et al. 2017) for the situations where the conical angle goes to zero and the bed becomes flat bottom.

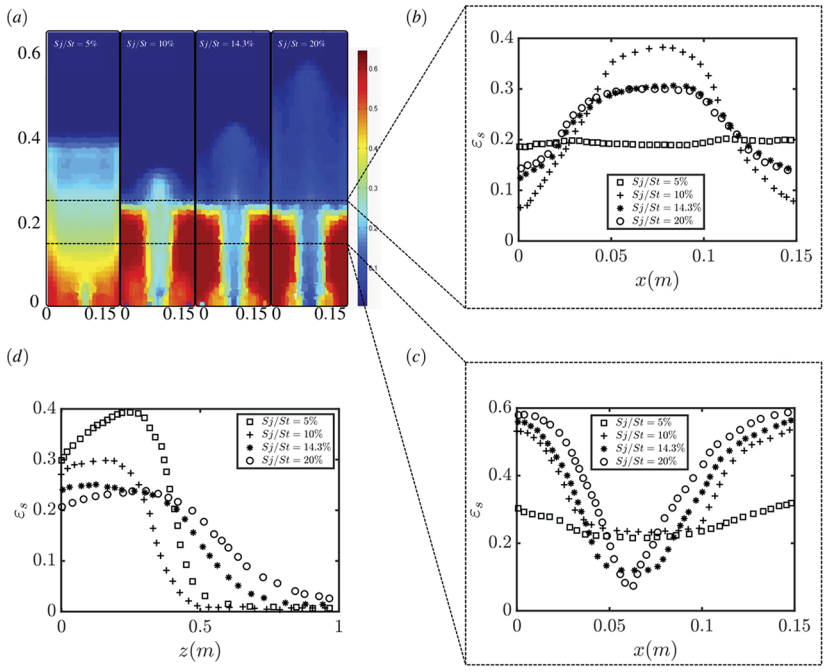


**Figure 7:** Solid volume fraction for different jet to bed cross-section ratios at constant temperature (a) contour plot at x = 0.042 m, solid volume fraction profile at (b) z = 0.25 m, (c) z = 0.15 m, and (d) x = 0.042 m.

The other parameter affected by jet to bed cross-section ratio is minimum spouting velocity. Until now several correlations have been presented in the literature to estimate the minimum spouting velocity. One of the most successful model is the one presented by (Mathur and Gishler 1955)

$$U_{ms,M-G} = \left(\frac{d_s}{S_T}\right)\left(\frac{S_j}{S_T}\right)^{\frac{1}{3}}\sqrt{\frac{2gL\left(\rho_s - \rho_g\right)}{\rho_g}} \tag{30}$$

as this model predicts and it is shown by the simulation results in Figure 8, at higher jet to bed cross-section the minimum spouting velocity increases at low temperatures. This situation may be explained by the point that at higher ratios, larger portion of the solid phase is exposed to the gas phase directly and energy of the gas phase distributed between larger number of particles. Therefore, the minimum spouting velocity increases. On the other hand, at high temperatures there is a discrepancy between what the model predicts and simulation results, in a sense that higher ratios result in lower minimum spouting velocities. The reason comes from the fact that at high temperatures the gas movement in the bed become more complicated and the model presented in (34) do not consider the flow pattern in the bed in derivation of the minimum spout velocity.

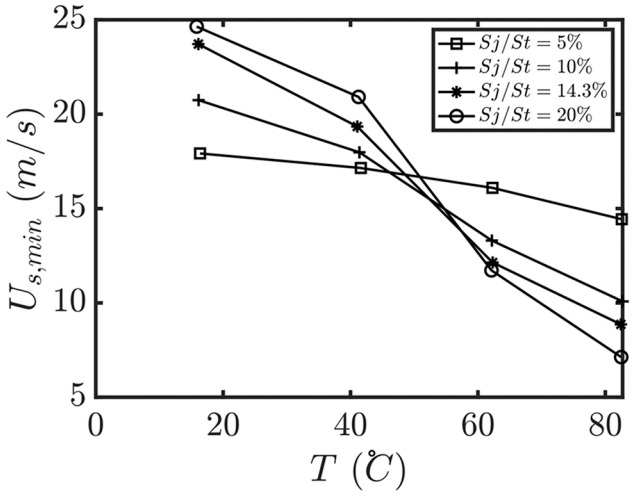


**Figure 8:** Variations of minimum spouting velocity versus temperature for different cross-section ratios.

## 3.4 Effect of inlet gas temperature

Another crucial parameter affecting the flow pattern in spout-fluid beds is the inlet gas temperature. Figure 9(a) and (b) show the z-component velocity of particles for Sj/St = 0.143 at z = 0.15 m and z = 0.25 m. As it is illustrated in these figures, increasing the inlet gas temperature results in higher particle velocity in the spout region. However, this effect is more significant at lower elevations in the bed. In the annulus region where the particle volume fraction is higher, the temperature does not affect the particle velocity crucially. This condition can be explained by the fact that due to higher particle volume fraction the heat transfer between gas-particle and particle-particle is higher and it just leads to small variations in drag forces and hence the particles velocity in this region. Besides, increasing the temperature decreases the gas density and augments its viscosity. Therefore, the drag force exerted to the solid particles increases. So, higher drag forc leads to larger particle velocity. In addition, comparing Figure 9(a) and (b) demonstrates that in spout region temperature variations has more significant effect in the regions near the gas inlet where the heat transfer deriving force is larger.

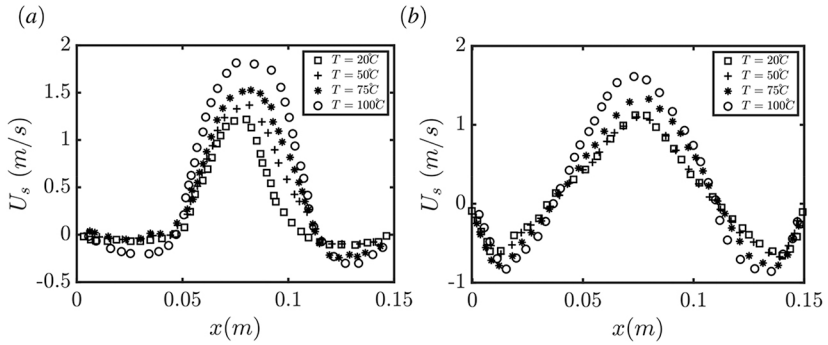


**Figure 9:** Z-component of particle velocity profile at different temperatures at (a) z = 0.15 m and (b) z = 0.25 m.

Gas inlet temperature also influences the pressure drop along the bed. Figure 10 shows that increasing the gas inlet temperature leads to higher pressure drop in the bed due to gas expansion and an increase in gas viscosity, this is consistent with what previously reported for Geldart D particles in a spouted bed (Hosseini et al. 2019; Wu, Guo, and Liu 2014). In addition, inlet gas temperature can affect the particle distribution in the bed. Figure 11 illustrates the time-averaged particle volume fraction at two elevations in the bed. At all temperatures, the minimum particle concentration happens in the middle of the bed that the gas velocity has its highest magnitude and by increasing the temperature this minimum moves towards higher values which may originates from the decline in particle lateral flux due to an increase in gas viscosity. At higher elevations in the bed the particle volume fraction becomes flat demonstrating less momentum exchange in these regions in comparison with vicinity of gas inlet which is compatible with the work recently published by (Patil, Peters, and Kuipers 2015; Wang et al. 2017; Zhou et al. 2019).

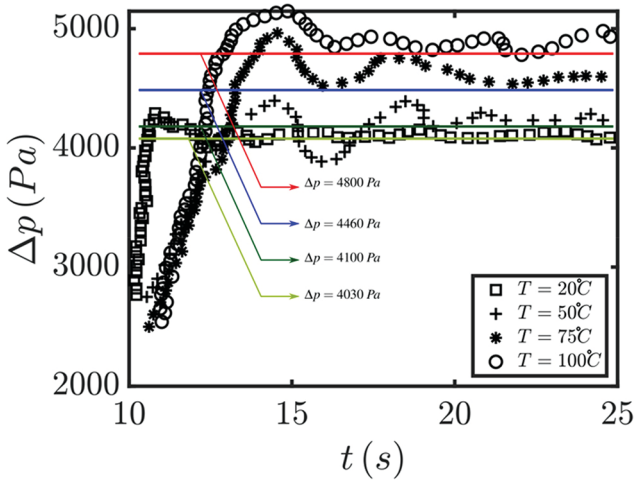


**Figure 10:** Pressure drop along the bed for various inlet gas temperatures from t = 10 s to t = 25 s. The colored horizontal lines represent the time-averaged pressure drop in the bed.

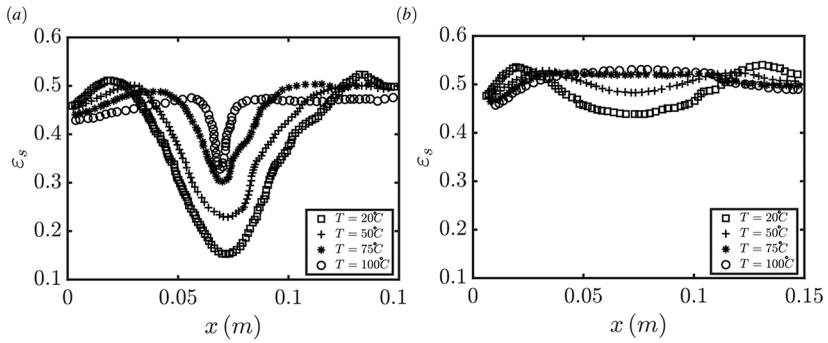


**Figure 11:** Effect of temperature on the solid volume fraction at two different heights in the bed (a) z = 0.15 m and (b) z = 0.25 m.

Finally, the time-averaged gas temperature distribution is examined in the bed as it is shown in Figure 12. By increasing the inlet gas temperature, the penetration length of the thermal energy increases along the bed and

hot gas can reaches to upper parts of the bed. It is worth to note that the heat transferred in lateral direction between gas and glass particles is smaller than that exchanged through convection mechanism along the bed ($k \sim 1 Wm^{-1}K^{-1}$). Furthermore, at higher temperatures some hot spots start to appear in the annulus region implying that the existence of recirculation in this region facilitate the heat transfer from spout to annulus region.

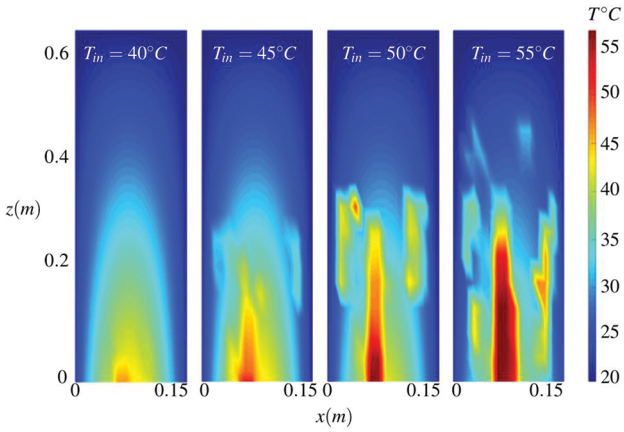


**Figure 12:** Time-averaged temperature contour plot at four different inlet gas temperatures.

## 4 Conclusion

Effects of jet to bed cross-section ratio and inlet gas temperature on the gas-solid flow behavior in a flat bottom spout-fluid bed have been investigated exploiting an Ansys-Fluent CFD code attempting to extend the previously reported study by (Link et al. 2008). The following concluding remarks were derived from the simulation results:

1. Jet to bed cross-section ratio can affect the gas-solid flow pattern significantly and change the boundary between the spout and annulus region. The fountain height in the bed can also be influenced mainly because of the variations in momentum exchange between the phases.

2. The minimum spouting velocity changes with altering the corss-section ratio in a way that for larger ratios the minimum spouting velocity becomes larger. This result is compatible with the existing models in the literature exploited to predict the minimum spouting velocity. However, at high temperature the simulation results are not compatible with the trend predicted by the models. This discrepancy may come from the fact that at high temperature local particle-particle interactions becomes more significant which cannot be captured in TFM model. Sufficient experimental works are necessary to understand the real trend of the minimum spouting velocity at high temperatures which is absent from the literature based on our knowledge.

3. Inlet gas temperature influences the hydrodynamics of the flow in the spout-fluid bed, it was shown that the particle velocity increases for higher temperatures and the pressure drop along the bed becomes larger either.

4. For higher gas inlet temperatures, thermal energy can reach to higher part of the bed and some hot spots start to exist in the annulus region.

### Acknowledgements

The authors would like to thank Sharif University of Technology (Tehran, Iran) and Okinawa Institute of Science and Technology Graduate University with subsidy funding from the Cabinet Office Government of Japan (Okinawa, Japan).

## Nomenclature

$\mathbf{v}$ Velocity $\left(\mathrm{ms}^{-1}\right)$

t Time (s)

P Pressure (Pa)

$\mathbf{g}$ Gravitational acceleration $\left(\mathrm{ms}^{-2}\right)$

$\mathbf{R_{gs}}$ Interaction force between gas and solid phases $\left(\mathrm{kgm}^{-2}\mathrm{s}^{-2}\right)$

$\bar{\bar{\mathrm{I}}}$ Identity matrix ()

$\mathrm{k}_{\theta\mathrm{s}}$ Diffusion coefficient of granular energy $\left(\mathrm{kgm}^{-1}\mathrm{s}^{-1}\right)$

$\mathrm{C_p}$ Specific heat $(\mathrm{kJmol}^{-1}\mathrm{K}^{-1})$

T Temperature (K)

H Heat transfer between phases $(\mathrm{kJmol}^{-1})$

$\mathrm{H_r}$ Reaction heat $(\mathrm{kJmol}^{-1})$

$\mathrm{k_g}$ Thermal conductivity $(\mathrm{Wm}^{-1}\mathrm{K}^{-1})$

Nu Nusselt number ()

Pr Prandtl number ()

$\mathrm{g_{0,ss}}$ Solid radial distribution function ()

$\mathrm{e_{ss}}$ Restitution coefficient ()

$\mathrm{D_{g,ij}}$ Rate of strain tensor for fluid phase $\left(\mathrm{s}^{-1}\right)$

Sj Jet cross-section area $(\mathrm{m}^2)$

St Total bed cross-section area $(\mathrm{m}^2)$

L Static bed height (m)

d Particle diameter (m)

$\mathrm{C_D}$ Drag coefficient ()

$\mathrm{I_{2D}}$ Second invariant of the deviatoric stress tensor ()

Greek letters

$\varepsilon$ Volume fraction ()

$\rho$ Density $\left(\mathrm{kgm}^{-3}\right)$

$\bar{\bar{\tau}}$ Stress tensor $\left(\mathrm{kgm}^{-1}\mathrm{s}^{-2}\right)$

$\theta$ Granular temperature $\left(\mathrm{m}^2\mathrm{s}^{-2}\right)$

$\varphi_{\mathrm{gs}}$ rate of pseudo-thermal energy dissipation $\left(\mathrm{kgm}^{-1}\mathrm{s}^{-3}\right)$

$\mu$ Solid phase granular viscosity (Pa.s)

$\emptyset$ Angle of internal friction ()

$\gamma_s$ Collisional dissipation of energy $(\mathrm{kg\ s}^{-3}\ \mathrm{m}^{-1})$

$\lambda_s$ Solid bulk viscosity $(\mathrm{kg\ s}^{-1}\ \mathrm{m}^{-1})$

Subscripts

g Gas phase

s Solid phase

## References


Agrawal, K., P. N. Loezos, M. Syamlal, and S. Sundaresan. 2001. "The Role of Meso-scale Structures in Rapid Gas-solid Flows." *Journal of Fluid Mechanics* 445: 151–85.

Behjat, Y., S. Shahhosseini, and S. H. Hashemabadi. 2008. "CFD Modeling of Hydrodynamic and Heat Transfer in Fluidized Bed Reactors." *International Communications in Heat and Mass Transfer* 35 (3): 357–68.

Carnahan, N. F., and K. E. Starling. 1969. "Equation of State for Nonattracting Rigid Spheres." *Journal of Chemical Physics* 51 (2): 635–&.

Correia, R., B. B. Paulo, A. S. Prata, and A. D. Ferreira. 2019. "Fluid Dynamics Performance of Phase Change Material Particles in a Wurster Spout-fluid Bed." *Particuology* 42: 163–75.

de Freitas, L. A. P. 2019. "Pharmaceutical Applications of Spouted Beds: A Review on Solid Dosage Forms." *Particuology* 42: 126–36.

Du, W., X. J. Bao, J. Xu, and W. S. Wei. 2006. "Computational Fluid Dynamics (CFD) Modeling of Spouted Bed: Assessment of Drag Coefficient Correlations." *Chemical Engineering Science* 61 (5): 1401–20.

Du, W., J. Xu, W. S. Wei, and X. J. Bao. 2013. "Computational Fluid Dynamics Validation and Comparison Analysis of Scale-up Relationships of Spouted Beds." *Canadian Journal of Chemical Engineering* 91 (11): 1746–54.

Duangkhamchan, W., F. Ronsse, F. Depypere, K. Dewettinck, and J. G. Pieters. 2010. "Comparison and Evaluation of Interphase Momentum Exchange Models for Simulation of the Solids Volume Fraction in Tapered Fluidised Beds." *Chemical Engineering Science* 65 (10): 3100–12.

Fattahi, M., S. H. Hosseini, and G. Ahmadi. 2016. "CFD Simulation of Transient Gas to Particle Heat Transfer for Fluidized and Spouted Regimes." *Applied Thermal Engineering* 105: 385–96.

Gamwo, I. K., J. S. Halow, D. Gidaspow, and R. Mostofi. 2003. "CFD Models for Methanol Synthesis Three-phase Reactors: Reactor Optimization." *Chemical Engineering Journal* 93 (2): 103–12.

Hosseini, S. H., M. Fattahi, and G. Ahmadi. 2015. "Hydrodynamics Studies of a Pseudo 2D Rectangular Spouted Bed by CFD." *Powder Technology* 279: 301–09.

Hosseini, S. H., M. Karami, H. Altzibar, and M. Olazar. 2019. "Prediction of Pressure Drop and Minimum Spouting Velocity in Draft Tube Conical Spouted Beds Using Genetic Programming Approach." *Canadian Journal of Chemical Engineering* 98 (2): 583–9.

Johnson, P. C., and R. Jackson. 1987. "Frictional-Collisional Constitutive Relations for Granular Materials, with Application to Plane Shearing." *Journal of Fluid Mechanics* 176: 67–93.

Link, J. M., N. G. Deen, J. A. M. Kuipers, X. Fan, A. Ingram, D. J. Parker, … J. P. K. Seville. 2008. "PEPT and Discrete Particle Simulation Study of Spout-fluid Bed Regimes." *Aiche Journal* 54 (5): 1189–202.

Lun, C. K. K., S. B. Savage, D. J. Jeffrey, and N. Chepurniy. 1984. "Kinetic Theories for Granular Flow - Inelastic Particles in Couette-Flow and Slightly Inelastic Particles in a General Flowfield." *Journal of Fluid Mechanics* 140 (March): 223–56.

Mathur, K. B., and P. E. Gishler. 1955. "A Technique for Contacting Gases with Coarse Solid Particles." *Aiche Journal* 1 (2): 157–64.

Moliner, C., F. Marchelli, L. Ong, A. Martinez-Felipe, A. Van der Dominic, and E. Arato. 2019. "Sensitivity Analysis and Validation of a Two Fluid Method (TFM) Model for a Spouted Bed." *Chemical Engineering Science* 207: 39–53.

Patil, A. V., E. A. J. F. Peters, and J. A. M. Kuipers. 2015. "Computational Study of Particle Temperature in a Bubbling Spout Fluidized Bed with Hot Gas Injection." *Powder Technology* 284: 475–85.

Saidi, M., H. B. Tabrizi, and J. R. Grace. 2019. "A Review on Pulsed Flow in Gas-solid Fluidized Beds and Spouted Beds: Recent Work and Future Outlook." *Advanced Powder Technology* 30 (6): 1121–30.

Santos, K. G., V. V. Murata, and M. A. S. Barrozo. 2009. "Three-Dimensional Computational Fluid Dynamics Modelling of Spouted Bed." *Canadian Journal of Chemical Engineering* 87 (2): 211–19.

Savari, C., R. Sotudeh-Gharebagh, G. Kulah, M. Koksal, and N. Mostoufi. 2019. "Detecting Stability of Conical Spouted Beds Based on Information Entropy Theory." *Powder Technology* 343: 185–93.

Schaeffer, D. G. 1987. "Instability in the Evolution Equations Describing Incompressible Granular Flow." *Journal of Differential Equations* 66 (1): 19–50 0022–0396.

Setarehshenas, N., S. H. Hosseini, M. N. Esfahany, and G. Ahmadi. 2017. "Three-dimensional CFD Study of Conical Spouted Beds Containing Heavy Particles: Design Parameters." *Korean Journal of Chemical Engineering* 34 (5): 1541–53.

Walsh, F. C., and C. P. de Leon. 2018. "Progress in Electrochemical Flow Reactors for Laboratory and Pilot Scale Processing." *Electrochimica Acta* 280: 121–48.

Wang, S. Y., R. C. Tian, H. L. Li, X. Q. Li, X. Wang, J. Zhao, … Q. J. Sun. 2017. "Predictions of Granular Temperatures of Particles in a Flat Bottomed Spout Bed." *Powder Technology* 322: 147–58.

Wang, S. Y., L. Q. Zhao, C. S. Wang, Y. S. Liu, J. S. Gao, Y. Liu, and Q. L. Cheng. 2014. "Numerical Simulation of Gas-solid Flow with Two Fluid Model in a Spouted-fluid Bed." *Particuology* 14: 109–16.

Wang, X., S. Y. Wang, R. C. Tian, R. C. Wang, L. L. Liu, Q. J. Sun, and J. W. Fan. 2018. "Numerical Study on Flow Behavior of Multi-component Particles in a Fluidized Bed Using a TFM-DEM Hybrid Model." *Powder Technology* 338: 795–805.

Wu, F., J. H. Bai, J. J. Zhang, W. J. Zhou, and X. X. Ma. 2019. "CFD Simulation and Optimization of Mixing Behaviors in a Spouted Bed with a Longitudinal Vortex." *Acs Omega* 4 (5): 8214–21.

Wu, M., Q. J. Guo, and L. Y. Liu. 2014. "Hydrodynamic Performance of a Spout-Fluid Bed with Draft Tube at Different Temperatures." *Industrial & Engineering Chemistry Research* 53 (5): 1999–2010.

Yang, S. L., K. Luo, M. M. Fang, and J. R. Fan. 2013. "Discrete Element Simulation of the Hydrodynamics in a 3D Spouted Bed: Influence of Tube Configuration." *Powder Technology* 243: 85–95.

Zhong, W. Q., X. J. Liu, J. R. Grace, N. Epstein, B. Ren, and B. S. Jin. 2013. "Prediction of Minimum Spouting Velocity of Spouted Bed by Cfd-Tfm: Scale-Up." *Canadian Journal of Chemical Engineering* 91 (11): 1809–14.

Zhou, G. W., W. Q. Zhong, A. B. Yu, and J. Xie. 2019. "Simulation of Coal Pressurized Pyrolysis Process in an Industrial-scale Spout-fluid Bed Reactor." *Advanced Powder Technology* 30 (12): 3135–45.